Volume 13
Number 34
14 September 2025
Pages 10375–10688

Journal of Materials Chemistry B

Materials for biology and medicine

rsc.li/materials-b

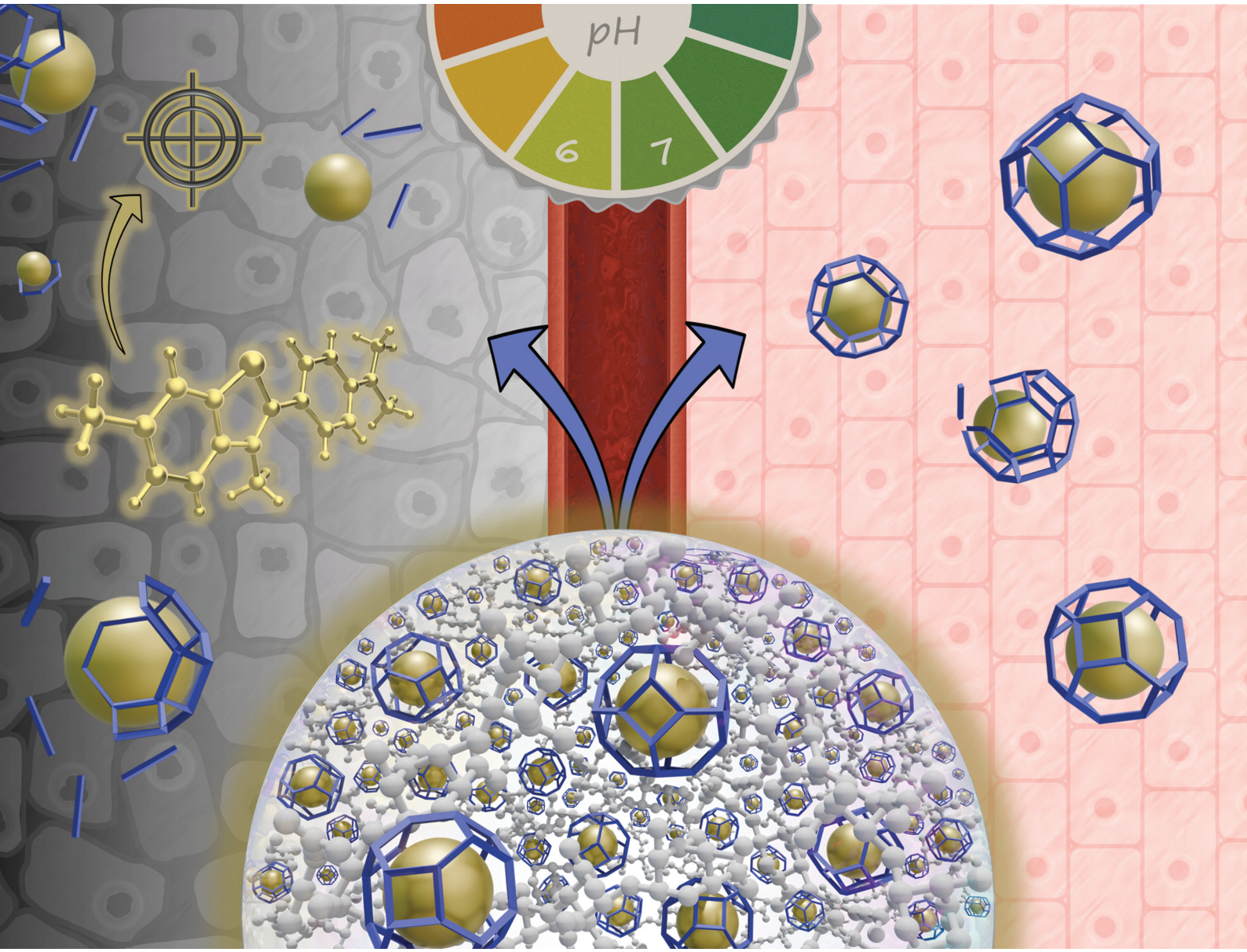

ISSN 2050-750X

ROYAL SOCIETY OF CHEMISTRY

PAPER

Roland A. Fischer, Angela Casini, Romy Ettlinger *et al.*
Design and characterisation of ZIF-8/alginate composites as drug carrier systems

Journal of Materials Chemistry B

ROYAL SOCIETY OF CHEMISTRY

PAPER

View Article Online
View Journal | View Issue

Cite this: J. Mater. Chem. B, 2025, 13, 10475

Design and characterisation of ZIF-8/alginate composites as drug carrier systems†

Sarah V. Dummert, ‡[a] Sylvia Dörschmidt, ‡[a] Theresa Bloehs, [a] Katia Rodewald,[b] Miriam Caviglia,[c] Claudia Schmidt,[c] Mian Zahid Hussain, [a] Julien Warnan, [a] Roland A. Fischer, *[a] Angela Casini *[c] and Romy Ettlinger *[a]

Metal–organic frameworks (MOFs) are promising candidates for drug carrier systems due to their high porosity and tuneable structures, however, their clinical translation is restrained. Integrating MOFs into processable matrices improves mechanical properties, processability, and often drug delivery performance. Hydrogels, as soft, three-dimensional polymer networks with high flexibility and biocompatibility, are particularly favourable candidates for advanced MOF-based drug carriers. However, a lack of fundamental material studies limits full exploitation of the potential and hinders further development of such composites. To address this, this study provides a physicochemical investigation of MOF/alginate hydrogels using ZIF-8 as a benchmark MOF and thioflavin T (ThT) as a model drug. A rapid, *in situ* encapsulation approach enabled the fabrication of ThT@ZIF-8 (14.2 wt% loading), which was incorporated into an alginate matrix (ThT@ZIF-8@Alg) at 95 wt%, putting MOF carrier functionality in a processable form. Characterisation including X-ray diffraction, infrared and diffuse-reflectance UV/Vis spectroscopy, and electron microscopy enabled a detailed investigation of MOF properties in the composite and confirmed its retained structural integrity. Drug release studies of ThT@ZIF-8@Alg closely mirrored the pure MOF's pH-triggered behaviour. Furthermore, by comparing different methods of incorporating ThT in (ZIF-8@)Alg matrices, we demonstrate the versatility of such composites in achieving customisable release profiles. *In vitro* preliminary studies of the antiproliferative activity of ThT@ZIF-8@Alg in cancerous and non-tumorigenic cells support the idea of sustained controlled release of ThT over 72 h at pH 7.4. This strategy advances MOF-hydrogel-based drug delivery systems, with potential applications in topical treatments and implant coatings.

Received 18th March 2025,
Accepted 24th June 2025

DOI: 10.1039/d5tb00614g

rsc.li/materials-b

Introduction

Biomedical research has advanced rapidly in recent years, driven by the increasing complexity of diseases, the understanding of their biomolecular mechanisms, and the need for innovative healthcare solutions. One area that has garnered considerable attention is drug delivery systems (DDS), which aim to enhance the efficacy and safety of therapeutic agents facilitating their patient compliance. Moreover, as therapeutic modalities expand beyond small molecules to include nucleic acids, peptides, proteins, and antibodies, DDS must be adapted to address new demands.[1,2]

Given these challenges, metal–organic frameworks (MOFs) offer a promising platform to overcome problems faced by other nanocarriers, which often suffer from poor formulation stability, low drug loading efficiencies or a lack of control over release rates.[3–9] MOFs, as solid-state coordination polymers with open framework structures, comprise metal nodes (ions or clusters) connected by multitopic organic ligands, offering remarkable versatility in composition, functionalization, and pore architecture.[6,10–12] The porosity and large internal surface areas of MOFs have driven interest in their biomedical applications, with a considerable step forward in the field marked by the transition from laboratory research to first clinical trials in 2023.[13] Their selective and high adsorption capacity for a plethora of active drug agents is one of the key features that

[a] Chair of Inorganic and Metal–Organic Chemistry, Department of Chemistry, TUM School of Natural Sciences, Technical University of Munich, Lichtenbergstraße 4, 85748 Garching, Germany. E-mail: romy.ettlinger@tum.de
[b] WACKER-Chair of Macromolecular Chemistry, Department of Chemistry, TUM School of Natural Sciences, Technical University of Munich, Lichtenbergstraße 4, 85748 Garching, Germany
[c] Chair of Medicinal and Bioinorganic Chemistry, Department of Chemistry, TUM School of Natural Sciences, Technical University of Munich, Lichtenbergstraße 4, 85748 Garching, Germany

† Electronic supplementary information (ESI) available. See DOI: https://doi.org/10.1039/d5tb00614g

‡ These authors contributed equally.

make MOFs particularly attractive for DDS.[14–17] However, while several lipid- and polymer-based drug delivery systems are in clinical trials or have already reached the market, MOFs are trailing behind.[18–20]

Alongside other factors, this can be attributed to limitations associated with pure MOF powders, such as poor mechanical properties. By combining MOFs with processable polymer matrices, materials with improved drug loading capacities, release kinetics, and targeting capabilities have been developed,[21–23] ranging from oral formulations to injectable depots, transdermal patches and tissue engineering.[24–32] Apart from synergistic property enhancement, the association of MOFs with polymers leverages their more established stand as drug delivery platforms. In this regard, incorporating MOFs into hydrogels—a class of soft, three-dimensional polymer networks with high water content and flexibility—offers complementary benefits,[33,34] with the hydrogel serving as a MOF reservoir for controlled release of therapeutic payloads, and the MOFs enhancing the hydrogel's mechanical properties and stability.[34–36] Among the various options of hydrogel-forming polymers, alginate particularly stands out.[33] The natural polysaccharide forms hydrogels through cross-linking with divalent cations in a straightforward and well-controllable manner. Alginate hydrogels are highly biocompatible and biodegradable, their structure resembling extracellular matrices of living tissues.[37–39] While some studies have tapped into the potential of MOF/alginate hydrogels for drug delivery, sensing, and wound healing, research has largely been driven by specific target applications rather than a comprehensive understanding of the fundamental properties of these hybrid materials.[40–43] Key aspects that require further investigation include a comparative investigation of MOF and drug incorporation modes, ambidexterity of functional material and hydrogel matrix, and detailed analysis of the role of MOFs as carriers and how they are impacted by hybridization.

In this study, we provide an in-depth physicochemical investigation of MOF/alginate hydrogels as drug delivery platforms. The main focus is to provide structural and chemical characterization of MOF/hydrogel composites, addressing a gap in the literature where such properties are often overlooked in favour of biological endpoints. Assessing the MOF's effect in the matrix, key design strategies are identified to tailor these materials for specific carrier applications.

For this purpose, we intentionally chose well-characterized pristine materials to limit the variability of the unknowns in the resulting composite. Thus, ZIF-8 (ZIF = zeolitic imidazolate framework) is used as a benchmark MOF composed of zinc nodes and 2-methylimidazole linkers, featuring a highly porous structure with size-amendable cavities.[44] ZIF-8 is thermally and chemically stable, and can be synthesized under mild conditions within minutes.[45] Moreover, it exhibits good biocompatibility and has previously been used to encapsulate a wide range of drugs, from small molecules to proteins.[46–50] Here, we use the benzothiazole dye thioflavin T (ThT) as a model drug, a widely used 'gold standard' for selectively staining and to identify amyloid fibrils.[51,52] As a strongly absorbing dye ('basic yellow', $\lambda_{max,abs.}$ = 412–413 nm),[53,54] it is easily traceable (detection limit: <0.1 μg mL^{-1}). A fast, *in situ* encapsulation approach to obtain the drug-loaded MOF, denoted as ThT@ZIF-8, is presented. Using an automated method, ThT@ZIF-8 was brought into an alginate matrix, resulting in composite materials (ThT@ZIF-8@Alg) with uniform shape and homogeneous properties. Both materials were thoroughly characterized, including X-ray diffraction, UV/Vis spectroscopy, scanning electron microscopy, gas sorption measurements and infrared spectroscopy. Composites were fabricated with a ZIF-8 and ThT content of 95 wt% and 13.5 wt%, respectively, with pristine MOF properties and drug carrier performance retained while offering a processable, shaped, macroscopic format. Through studies of four different drug incorporation strategies to (MOF@)alginate matrices and follow-up release experiments, the role of ZIF-8 as a protective shell for the drug and in achieving high payloads is highlighted. With the drug@MOF synthesis decoupled from a facile composite fabrication method, an auspicious approach for the development of tailorable MOF/hydrogel materials for biomedical applications is offered.

Results and discussion

Encapsulation of ThT in ZIF-8

The synthesis of pristine ZIF-8 as well as the one-pot encapsulation of ThT in ZIF-8 (ThT@ZIF-8) were carried out in water and at room temperature within minutes, using a modified previously reported strategy.[55] To optimise the ThT loading capacity, different synthesis approaches and reaction parameters were screened, namely *in situ* co-crystallisation and post-synthetic impregnation with different concentrations of ThT in solution, as outlined in the ESI† (Section S3). Ultimately, ThT@ZIF-8 was obtained from a room-temperature one-pot synthesis, by adding an aqueous solution of 2-methylimidazole and ThT to a solution of zinc nitrate and sodium hydroxide as base and modulator in water, leading to instantaneous precipitation of the phase-pure product in high yield. Additionally, pristine ZIF-8 was synthesised following the same route while excluding ThT from the reaction solution.

The synthesised MOFs show characteristic reflections at 2θ values of 7.4° (110), 10.5° (200) and 12.8° (211) in the powder X-ray diffraction (PXRD) patterns, matching with the reported diffractogram (CCDC: 864309) and thus confirming the successful synthesis of ZIF-8 and ThT@ZIF-8 (Fig. 1a).[56] For the latter, a colour change of the originally white MOF powder to yellow was observed. This is evidenced by the diffuse-reflectance ultraviolet-visible (DR-UV/Vis) spectra (Fig. 1b) of both species. While ZIF-8 shows absorbance only <250 nm, ThT@ZIF-8 exhibits two additional bands at 423 and 298 nm, in line with that of ThT. The strongly absorbing dye shows a DR-UV/Vis main absorption band at 423 nm in pristine state, however, upon changing the pH, the ThT absorption spectrum is known to undergo significant reversible changes. In basic solutions, the intensity of the main absorption band decreases while the intensity of the weaker band at $\sim$300 nm increases, caused by hydroxylation of the carbon in the thiazole

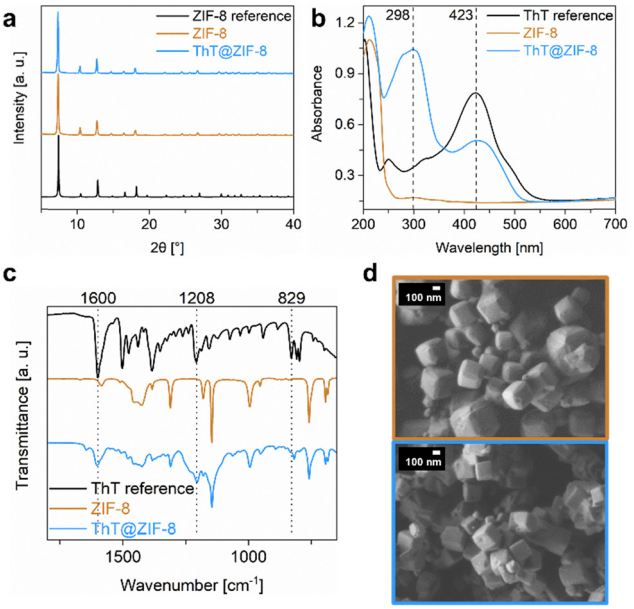

Fig. 1 (a) PXRDs of ZIF-8 (brown), ThT@ZIF-8 (blue) and a reference pattern of ZIF-8 (black, CCDC: 864309),[52] (b) DR-UV/Vis spectra of ZIF-8, ThT@ZIF-8 and ThT powder as reference (black), (c) FTIR spectra shown from 1800 to 650 cm^{-1} of ZIF-8, ThT@ZIF-8 and ThT powder as reference, (d) SEM images of ZIF-8 (top) and ThT@ZIF-8 (bottom).

group.[57–59] This effect is also visible in the DR-UV/Vis spectrum of ThT@ZIF-8, with the peak at 298 nm stronger than that at 423 nm, which can be ascribed to the basic nature of the pore environment in ZIF-8.[44,60] The successful encapsulation of ThT is further confirmed in the Fourier-transform infrared (FTIR) spectrum of ThT@ZIF-8 (Fig. 1c, full spectra shown in Fig. S4, ESI†). Three distinct ThT signals are observed at 1600 cm^{-1} (C=C stretching), 1208 cm^{-1} (C_{benz}–H stretching), and 829 cm^{-1} (C_{benz}–H bending), alongside the ZIF-8 bands. Additionally, several weaker ThT signals are overlapping with the MOF spectrum, particularly in the region between 1600 and 1200 cm^{-1}. The absence of significant shifts of ZIF-8 bands suggests that there are no strong interactions between the guests and the host, *e.g.*, at the nodes. Interestingly, the presence of ThT during ZIF-8 synthesis affected the crystal morphology, as observed in the scanning electron microscopy (SEM) images in Fig. 1d. Similar to previously-described structure-directing agents,[61,62] ThT shows a modulating effect, changing the rhombic dodecahedral crystals of pristine ZIF-8 (top picture) towards cubic shapes of ThT@ZIF-8 crystals (bottom picture), as well as reducing the average size from ~200–400 nm to ~100–300 nm. To visualise the particle size distribution of ThT@ZIF-8, transmission electron microscopy (TEM) images were recorded and analysed, showing an average crystal size of 103 ± 40 nm (Fig. S5, ESI†). To further confirm the successful encapsulation and molecular integrity of ThT in ZIF-8, ^{1}H nuclear magnetic resonance (NMR) spectra were recorded after digestion of ThT@ZIF-8 in DMSO-d_6 and DCl. The signals of both organic components of the material, 2-methylimidazole and ThT, can be identified in the ^{1}H-NMR, as shown in Fig. S6 (ESI†). The ThT loading in ThT@ZIF-8 was quantified to be 14.2 wt% *via* solution ultraviolet-visible (UV/Vis) spectroscopy after digestion of ThT@ZIF-8 in diluted acetic acid, for which details and the calibration curve can be found in the ESI† (Section S2 and Fig. S1). Based on this, a theoretical pore filling degree of ~19% and ThT loading of ~0.74 molecules per pore can be estimated (eqn (S1) and (S2), ESI†). Considering the ZIF-8 pore size relative to ThT's dimensions, the theoretical ThT loading per pore falls within an expected range. Since ThT is too large (3–4 Å × 15–16 Å) to enter the pores of ZIF-8 (aperture: 3.4 Å, diameter: 11.6 Å, based on the ideal theoretical structure) post-synthetically, it can only be encapsulated in high amounts through co-crystallization during MOF formation, where the framework forms around the guest molecule and sterically traps it in the pores.[60,63] This aligns with the above-mentioned synthesis screening reactions (ESI,† Section S3), which showed that only negligible ThT loading could be achieved *via* an impregnation approach, and increasing ThT concentrations in the one-pot reactant solution beyond a certain point (10 mg mL^{-1}) did not result in loadings higher than 14.2 wt%. Thermogravimetric analysis (TGA) of ThT@ZIF-8 shows an initial loss of residual solvent, then decomposition of ThT starting at ~75 °C, followed by degradation of the ZIF-8 structure from ~350 °C onwards, which is in agreement with literature reports (Fig. S7, ESI†).[64] From the residual masses at 800 °C (ZIF-8: 33.0%, ThT@ZIF-8: 29.1%, ThT: 2.1%), a ThT loading of 12–13 wt% can be estimated, which is in line with the loading determined *via* UV/Vis. Gas sorption isotherms (N_2, 77 K) recorded of ThT@ZIF-8 (Fig. S8, ESI†) show the typical Type I shape of microporous ZIF-8.[44,65] In comparison with pristine ZIF-8, a reduction of N_2 uptake from 533 to 463 cm^3 g^{-1} (13%) and of the calculated Brunauer–Emmett–Teller (BET) specific surface area from 1678 to 1554 m^2 g^{-1} (8%) was observed in ThT@ZIF-8. Notably, the pore size distribution (PSD) (Fig. S9, ESI†) reflects the incorporation of ThT with a reduction of 17% of the available pore volume, which aligns well with the theoretical degree of pore filling calculated from the loading obtained from UV/Vis analysis.

ThT@ZIF-8@Alg composite fabrication

Following the successful synthesis of ThT@ZIF-8, hybridisation of the MOF with sodium alginate (SA) was pursued. Inspired by the work of Queen *et al.*,[66] these composites were obtained by making a homogeneous dispersion of MOF and SA powder in water, which was then dropped into an aqueous curing solution of calcium chloride. To determine optimal MOF/SA/Ca^{2+} ratios for composite fabrication with maximum MOF incorporation, initial experiments were manually conducted using pristine ZIF-8 (see ESI,† Section S5). Ultimately, ZIF-8@Alg was successfully formed from a slurry containing 95 wt% MOF, achieving remarkable MOF content (Fig. S10 and S11, ESI†). Instantaneous cross-linking of the alginate chains by Ca^{2+} upon contact with the curing solution triggers the direct polymerisation of the alginate around the MOF and leads to the formation of stable spherical beads, which effectively retain the MOF particles within the matrix. This can be attributed not only to physical entrapment within the crosslinked polymer network but also to

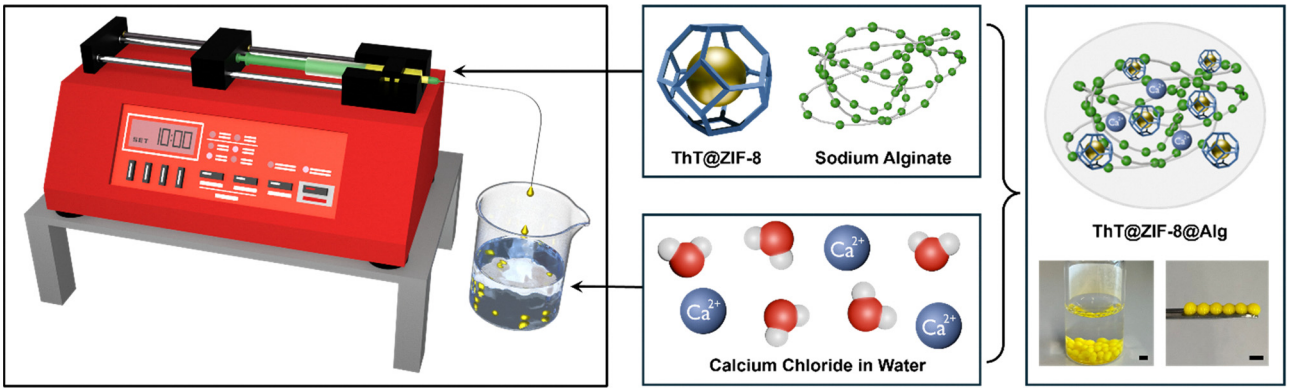

Scheme 1 Schematic representation of the syringe pump setup for automated fabrication of ThT@ZIF-8@Alg beads with a uniform shape and size. A syringe filled with aqueous ThT@MOF/SA dispersion is fixed on a syringe pump and the content is steadily dropped into a Ca^{2+} curing solution, upon which the spherical beads are formed; scale bar = 2 mm.

interactions between the MOF and alginate. Previous studies have shown that alginate coordinates to MOF metal nodes *via* carboxylate groups, while additional stabilization arises from non-covalent interactions between the alginate chains and the MOF linkers.[66,67] These combined interactions contribute to the enhanced mechanical robustness and structural integrity of the composite compared to the individual components.[34,40,68]

Building on these initial screenings, alginate composites were made with ThT-loaded ZIF-8 (denoted as ThT@ZIF-8@Alg), with a theoretical ThT@ZIF-8 and ThT content of 95 wt% (0.68 mg per bead) and 13.5 wt% (<0.10 mg per bead), respectively. To partially automate the shaping process, composite fabrication was performed using a syringe pump setup, as shown in Scheme 1. Dropping the MOF/SA dispersion into the Ca^{2+} curing solution at a constant speed and with a fixed volume yielded beads of a uniform shape and size (spherical, diameter: ~1.8 cm), with their homogeneity facilitating further material studies. Furthermore, this setup allows a more expeditious and highly reproducible formation of larger amounts than a manual procedure. For this purpose, an aqueous MOF/SA dispersion was filled into the syringe and the flowrate was adjusted to maintain efficient dropping from a fixed height. Additionally, a beaker filled with the curing solution was placed under the outlet of the syringe needle and carefully stirred to collect the formed beads. Their size and weight before and after drying is documented in Table S5 (ESI†). After washing with water, the beads can be dried under ambient atmosphere.

Following the successful development of a fabrication method for the beads, the potential benefit of using of a MOF as drug carrier was investigated. To do this, the influence of different methods of incorporating ThT in alginate polymers was tested by four different strategies overall: (i) beads with pre-loaded ThT@ZIF-8 (ThT@ZIF-8@Alg, type I), (ii) beads with pristine ZIF-8 and post-synthetic impregnation with ThT (ZIF-8@Alg-ThT, type II), (iii) beads without MOF only using ThT and alginate (ThT@Alg, type III) and (iv) beads without MOF and post-synthetic impregnation with ThT (Alg-ThT, type IV). All methods are described in detail in the ESI† (Section S6). Scheme 2 shows microscope images of all types of beads as well

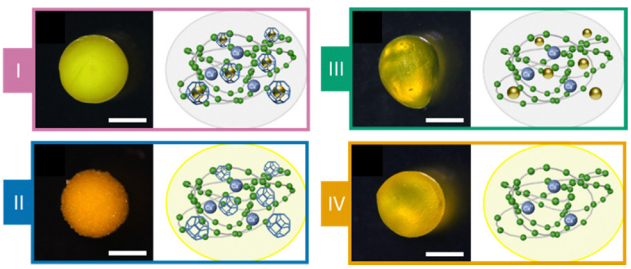

Scheme 2 Light microscope images and schematic representations of type I–IV beads (scale bar: 1 mm).

as their schematic representations. These reveal visual differences regarding their colour intensities, ranging from opaque yellow for type I, opaque yellow-orange shade for type II with visible crystallites on the surface, and more transparent and less yellow beads for type III and IV. Furthermore, it is worth noting that, upon drying, type I and II beads (with ZIF-8), shrink to half their size (Table S5, ESI†), whereas Type III and IV beads (without ZIF-8) lose >90% of their initial volume as water is removed from the hydrogel, underlining how the presence of the MOF reinforces the structural integrity of the hydrogel.

The PXRD patterns of type I and type II beads demonstrate, that the MOF structure remains intact over the composite fabrication process (Fig. 2a). Without containing MOF, the type III and IV beads do not show any reflections. The DR-UV/Vis spectra show major differences of ThT absorbance within the different bead types (Fig. 2b). While the spectrum of type I is very similar compared to the material pre-processing, type II shows the main absorbance maximum around 423 nm which corresponds to pristine ThT. Most likely, this can be ascribed to the difference in the integration process. After impregnation, ThT is only distributed in the ZIF-8@Alg matrix and partially adsorbed on the surface of ZIF-8 crystals. Thus, while some effects of the MOF scaffold are visible, the influence is less pronounced compared to the interactions that occur within the pore. The type III and type IV beads both exhibit a broad absorbance from <250 to >500 nm, which indicates

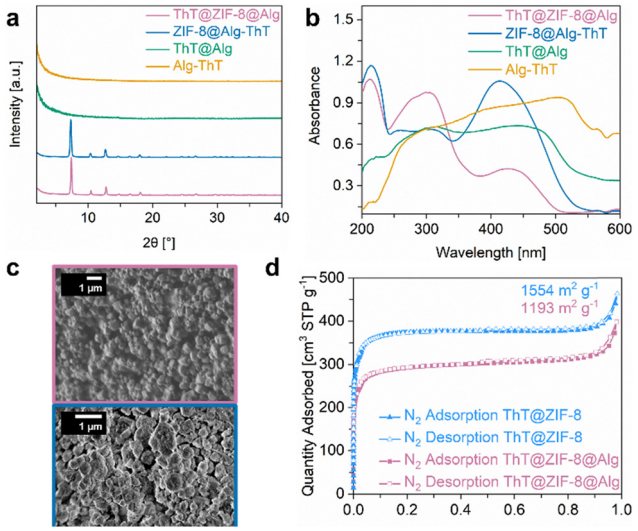

Fig. 2 (a) Stacked PXRDs of ThT@ZIF-8@Alg (violet), ZIF-8@Alg-ThT (dark blue), ThT@Alg (green) and Alg-ThT (orange), (b) DR-UV/Vis spectra of ThT@ZIF-8@Alg, ZIF-8@Alg-ThT, ThT@Alg and Alg-ThT, (c) SEM images of ThT@ZIF-8@Alg (top) and ZIF-8@Alg-ThT (bottom), (d) N_2 sorption isotherms (77 K) and calculated specific BET surface areas of ThT@ZIF-8 (light blue) and ThT@ZIF-8@Alg.

interactions of ThT with the alginate polymer and an increased number of possible electronic transitions. Since the alginate content is much higher than in type I and II beads (5 wt% *vs.* >50 wt%), such ThT-alginate interactions are likely more pronounced. The recorded FTIR spectra (Fig. S12 and S13, ESI†) and TGA curves (Fig. S14, ESI†) of type I–IV beads confirm these findings and can be found in the ESI.† In the SEM images of type I and II beads (Fig. 2c) ZIF-8 is clearly visible. While the MOF particles are homogeneously spread and visibly agglutinated in the alginate matrix in type I, the particles in type II slightly lost their distinct cubic morphology and show a rougher and more damaged surface. This is indicative of the MOF partially disintegrating during the impregnation in the weakly acidic ThT solution. Additional SEM pictures of other beads are given in the ESI† (Fig. S15).

The sorption isotherms (N_2, 77 K) of pristine ThT@ZIF-8 and Type I beads are compared in Fig. 2d, revealing N_2 uptake of 463 and 398 $cm^3\ g^{-1}$ and calculated specific BET surface areas of 1554 and 1193 $m^2\ g^{-1}$, respectively. That constitutes a slight reduction of N_2 uptake of 14% and a surface area loss of 23% upon composite fabrication. This reduction is somewhat higher than expected regarding the incorporation of the MOF in 5 wt% of an alginate hydrogel and might be attributed to the minimal particle modification upon processing. It is worth noting, that a mild activation temperature (70 °C) for the BET measurements was chosen to avoid thermal damage to the encapsulated drug and polymer matrix, which possibly did not lead to complete removal of residual guest molecules (*e.g.*, traces of water). PSD analysis of both materials (Fig. S16, ESI†) and comparison to the PSD of pristine ZIF-8 show a gradual reduction of the available pore volume from ZIF-8 (0.6789 $cm^3\ g^{-1}$) to ThT@ZIF-8 (0.5640 $cm^3\ g^{-1}$, 83% of ZIF-8), due to the encapsulation of ThT, and again from ThT@ZIF-8 to ThT@ZIF-8@Alg (0.4448 $cm^3\ g^{-1}$, 79% of ThT@ZIF-8), due to the encapsulation in the Alg matrix.

ThT release experiments

After preparation of the different (MOF) composite materials, precise analyses of the drug release properties were performed. Prior to this, the ThT loading was determined *via* solution UV/Vis monitoring of digested samples (for details see ESI,† Section S2 and Fig. S1). When ThT is encapsulated in ZIF-8 before combination with the alginate matrix (type I beads), its loading of 0.078 mg per bead is significantly higher than in the other three materials (Fig. 3a). Impregnation of ZIF-8@Alg or pristine Alg beads in a ThT solution (type II and type IV beads, respectively) yielded the same amount of loaded ThT (0.014 mg per bead); hence, the mere presence of the MOF without acting as a carrier does not have a substantial influence. This loading equals only 18% of that achieved in type I beads and appears to be primarily limited by the volume of the beads into which the ThT can diffuse. The lowest ThT loading was found in ThT@Alg (type III beads) with 0.011 mg per bead (14% compared to type I).

The stability of ThT@ZIF-8@Alg (type I beads) was investigated in different media over time and compared to the pristine ThT@ZIF-8 powder. One of the advantages of ZIF-8 in biomedical applications is its chemical stability in neutral and alkaline environments and resilience towards high ionic strength solutions, such as phosphate-buffered saline (PBS).[45,69] To verify the permanence of the materials used in this study, ThT@ZIF-8 and ThT@ZIF-8@Alg were immersed in deionised water (pH 6) or PBS (pH 7.4) for a week (see ESI,† Section S8) and the supernatants were monitored *via* UV/Vis. In deionised water, neither of the materials showed noteworthy ThT release even after seven days (Fig. S17, ESI†), which can be attributed to the high stability of ZIF-8 under these conditions. The fact that scaffold stability is retained in the composite as well further demonstrates that the composite fabrication has no negative influence on the MOF properties. In PBS (pH 7.4), both materials show minor ThT release after seven days (Fig. S18, ESI†) and slight decomposition of the MOF into zinc phosphate (Fig. S19 and S20, ESI†). The degradation of ThT@ZIF-8@Alg is

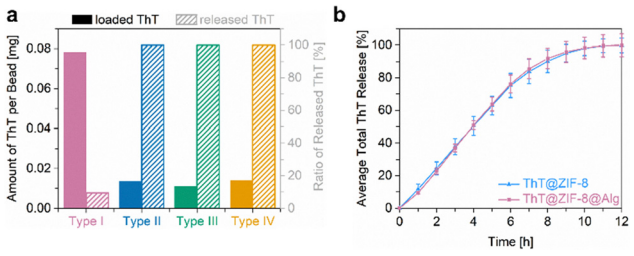

Fig. 3 (a) Comparison of amounts of ThT integrated in (left columns, filled) or released from (right columns, dashed) ThT@ZIF-8@Alg, ZIF-8@Alg-ThT, ThT@Alg and Alg-ThT beads, (b) Averaged release profiles of ThT from triplicate series of ThT@ZIF-8 and ThT@ZIF-8@Alg in PBS (pH 6). The ThT@ZIF-8@Alg curve was normalised to the ThT amount in solution.

somewhat more pronounced than that of ZIF-8@Alg, presumably since the crystals are well distributed and accessible in the Alg matrix and thus more exposed to the PBS than in crystalline agglomerates.

Exploiting the acid lability of ZIF-8 as a trigger for controlled drug release, a slightly acidic pH (6) was selected to mimic the environment of cancer tissues, and the release profile was monitored over time. For this purpose, ThT@ZIF-8 and ThT@ZIF-8@Alg were immersed in PBS buffer adjusted to pH 6, where the combination of acidity and ionic strength effects induced structure degradation of the MOF framework into the building units Zn^{2+} and 2-methylimidazole, and release of ThT. The ThT concentration in solution was monitored *via* UV/Vis absorption spectroscopy until ultimately all ThT@ZIF-8 had decomposed and ThT release was completed. To avoid that the basic nature of the MOF linkers neutralises the pH of the medium, therefore, halting ZIF-8 decomposition, the PBS (pH 6) was exchanged completely and replaced with fresh medium at one-hour intervals. The series of measurements was performed in triplicates and the corresponding averaged release profiles are displayed in Fig. 3b, with the amount of released ThT plotted against time. After 12 h, ThT@ZIF-8 had decomposed completely and released all previously encapsulated ThT, from both powder and composite form. Notably, the initial release profile (0–6 h) is approximately linear for both materials, averaging 12.5% per hour, and strikingly similar overall. Visibly, ThT is released in a controlled fashion and precise amounts due to acid-induced ZIF-8 decomposition, until an equilibrium point, where the medium is neutralised, and the release stops until an acidic environment is introduced again. This trend continues until ~75% of the initially present ThT is released (6 h), after which it gradually slows until MOF decomposition is complete and 100% release are reached. Due to the homogeneous distribution of ThT in ZIF-8 and a definitive response of ZIF-8 to the acid trigger, the release can be controlled meticulously. Remarkably, the ThT@ZIF-8@Alg composite mirrors the release profile of pristine ThT@ZIF, evidencing how strongly its material properties are retained in the alginate matrix and how the MOF phase governs the release mechanism.

Similarly, also the other three materials (type II, III, IV beads) were placed in PBS (pH 6) at 37 °C for one hour, after which the amount of released ThT was measured. Of the four, only type I beads showed a sustained ThT release with 9.4% of the total encapsulated amount found in the PBS supernatant, while all others (type II, III, IV beads) released all contained ThT (Fig. 3a). As previously observed, impregnation of ZIF-8 materials with a solution of ThT only leads to weak adsorption on the MOF surface. ThT cannot enter the pores of ZIF-8 post-synthetically and is easily removed upon washing. On the other hand, it is sterically trapped in the pores of ZIF-8 after one-pot synthesis. This ensures strong retention of ThT within the structure, allowing it to be released only when ZIF-8 decomposes – a process that can be controlled by a pH trigger. In contrast, when ThT is brought into the (ZIF-8@)Alg matrix without a protective cage, the interactions are much weaker, and its release is in the realm of diffusion control. This generally leads to decreased loadings, as ThT is washed out in the curing solution and/or during the product washing process (as evidenced by visible yellow colouration of the solutions), while the rest is released quickly from the matrix when brought in contact with the buffer. These findings highlight the benefits of the carefully built core@shell@matrix system in this study and serve as a proof-of-concept that high drug payloads and sustained release can be achieved only by a targeted, bottom-up strategy. On the other hand, rapid release of the active agent can be attained by loosely incorporating the drug into the alginate matrix, without a surrounding MOF scaffold.

Table 1 EC_{50} values of ThT, Tht@ZIF-8@Alg, ZIF-8, and ZIF-8@ThT after 72 h of incubation on human A549 adenocarcinoma alveolar basal epithelial cells and VERO E6 kidney epithelial cells. EC_{50} values in μM normalized for the ThT concentration, except that for ZIF-8 (μg mL^{-1}). Data represent mean ± standard deviation ($n \geq 3$)

	EC_{50} [μM]	
Compound	A549	VERO E6
Thioflavin T (ThT)	1.4 ± 0.1	31.1 ± 0.5
ThT@ZIF-8@Alg	21.3 ± 0.2	33.7 ± 0.7
ThT@ZIF-8	>44.5	>44.5
ZIF-8	>100[a]	>100[a]

[a] Values expressed in μg mL^{-1}.

Antiproliferative activity studies in cancer cells *in vitro*

Finally, preliminary studies on the antiproliferative activity of the composite beads ThT@ZIF-8@Alg was tested in human A549 lung cancer cells and in non-tumorigenic VERO E6 kidney epithelial cells *in vitro*. Cells were incubated with the material for 72 h. ThT and Tht@ZIF-8 were also tested for comparison. The EC_{50} values (half-maximal effective concentrations) were determined as the concentration that caused 50% inhibition of cell proliferation compared to untreated control. The data, reported in Fig. S21 (ESI†) and Table 1 represent the mean of three independent experiments. Fig. S21 (ESI†) shows the variation of cell viability as a function of the concentration of ThT (free or encapsulated). In the applied experimental conditions (pH 7.4), a slow release of ThT from the composite is to be expected over 72 h. This is indeed evidenced by the lower cytotoxic effect of the composite ($EC_{50/A549}$ = 21.3 ± 0.2 μM) *vs.* the free ThT (EC_{50} = 1.4 ± 0.1 μM). Moreover, the treatment maintained a certain selectivity for the cancerous cells over the VERO ones. Both ZIF-8 and ZIF-8@ThT did not show antiproliferative activity even at the highest tested concentrations in both cell lines.

Conclusions

In this study, ThT@ZIF-8 (14.2 wt% loading, ~0.74 molecules per ZIF-8 cage) was fabricated as a model system and brought into an alginate matrix to explore how versatile MOF/alginate composites for drug delivery systems can be designed effectively. The resulting composites can be endowed with a high

content of functional material and retain the intrinsic properties of the original drug@MOF inclusion compound while transforming it from a powder into a shapable material. This was demonstrated by the successful matrix incorporation of 95 wt% ThT@ZIF-8 to yield ThT@ZIF-8@Alg, which exhibited consistent, pH-triggered release behaviour closely mirroring that of the pristine ThT@ZIF-8, with an initial release rate of 12.5% h^{-1} that slowed after six hours. This approach of using a preformed drug@MOF inclusion compound was compared with alternative drug incorporation methods, revealing diffusion-based loading and release kinetics while demonstrating the versatility in designing such drug carriers. By selecting or combining these methods, release profiles can be adapted for sustained, stimuli-triggered, or rapid delivery.

Advancing the shaping method of well-defined drug@MOF@alginate carrier systems in the future, for example *via* 3D printing and thin-film fabrication is a vital step towards applications such as treatment of skin diseases, implant coatings, and others. In addition, the crosslinking ion in the curing solution could be exchanged to engineer the mechanic properties of the resulting hydrogel or offer multi-level functionality customisation.[70,71] By bridging the gap between tailored material design and functional biomedical applications, this method highlights a powerful pathway for advancing MOF-based drug carrier systems.

Looking at the vast diversity of adjustable parameters, such as nature of MOF, carrier-to-matrix ratios, choice of crosslinking ion during composite fabrication and conjugable methods of drug incorporation, the showcased concept can be tailored to multiple purposes, extending the applicability of MOF hydrogels beyond singular systems. Due to decoupling the design of the MOF as a drug carrier from its integration into the alginate matrix, this method allows for great latitude in drug@MOF synthesis, including the choice of building units, selective drug loading, tailoring of crystal size or integration of stimuli-responsiveness. It is worth noting that all materials used in this study were synthesised in aqueous media, thus, avoiding solvents detrimental to living organisms and the environment. Hybrid materials, such as proposed in this study, can surpass the limitations of purely organic or inorganic carriers by combining the strengths of both materials and thus, fulfil disease- and target-specific requirements that existing materials cannot attain.

Experimental

General information

All chemicals were purchased from commercial suppliers and used directly without additional treatment or purification. The ESI,† provides further details on all chemicals, syntheses, devices, and techniques used in this study.

Synthetic procedures

ZIF-8. In a 20 mL screw cap vial, 0.20 g $Zn(NO_3)_2{\cdot}6H_2O$ (0.67 mmol, 1.00 eq.) were dissolved in 0.8 mL deionised water *via* ultrasonication and the pH value was adjusted to 8 with 3.5 mL of 0.2 M NaOH (aq.). Then, a second solution of 2.00 g 2-methylimidazole (24.36 mmol, 36.36 eq.) in 12.0 mL deionised water was prepared *via* ultrasonication and added dropwise (~2 drops per second) to the first solution before the mixture was stirred (200 rpm) for 15 min at room temperature (21 °C). The precipitate was isolated by centrifugation (50 mL falcon tube, 7800 rpm, 10 min), washed with a mixture of EtOH and H_2O (v/v = 1 : 1, 3 × 20 mL) and dried at 50 °C in an oven, yielding ZIF-8 (0.16 g, >99% yield with respect to $Zn(NO_3)_2{\cdot}6H_2O$) as a white powder. For sorption measurements, the obtained product was activated under vacuum (1×10^{-3} mbar) at 70 °C for 12 h.

ThT@ZIF-8. In a 20 mL screw cap vial, 0.20 g $Zn(NO_3)_2{\cdot}6H_2O$ (0.67 mmol, 1.00 eq.) were dissolved in 0.8 mL deionised water *via* ultrasonication and the pH value was adjusted to 8 with 3.5 mL of 0.2 M NaOH (aq.). Then, a second solution of 2.00 g 2-methylimidazole (24.36 mmol, 36.36 eq.) and 0.12 g thioflavin T (0.37 mmol, 0.55 eq.) in 12.0 mL deionised water was prepared *via* ultrasonication and added dropwise (~2 drops per second) to the first solution before the mixture was stirred (200 rpm) for 15 min at room temperature (21 °C). The precipitate was isolated by centrifugation (50 mL falcon tube, 7800 rpm, 10 min), washed with a mixture of EtOH and H_2O (v/v = 1 : 1, 3 × 20 mL) and dried at 50 °C, yielding ThT@ZIF-8 (0.13 g, 82% yield with respect to $Zn(NO_3)_2{\cdot}6H_2O$) as a yellow powder. For sorption measurements, the obtained product was activated under vacuum (1×10^{-3} mbar) at 70 °C for 12 h.

ZIF-8@Alg and ThT@ZIF-8@Alg beads. In a 20 mL screw cap vial, 0.51 g of finely ground ZIF-8 or ThT@ZIF-8 powder were dispersed in 5.0 mL Milli-Q® water by stirring at room temperature (21 °C) for 1 h with intermittent ultrasonication periods (~2 min, every 15 min). After the MOF powder was well dispersed, 0.03 g of sodium alginate were added and the resulting mixture was again stirred at room temperature for 3 h with intermittent ultrasonication periods (~2 min, every 30 min). Once a homogenous, viscous dispersion was obtained, the mixture was filled into a 20 mL Luer Lock syringe capped with a needle (21G, 0.8 × 120 mm) and dropped into a carefully stirred solution of $CaCl_2$ (anhy.) in Milli-Q® water (20 mg mL^{-1}) at constant speed (~1 drop per 2 seconds) using a syringe pump. After 5 min, the formed ZIF-8@Alg or ThT@ZIF-8@Alg composite beads were separated from the curing solution *via* filtration, washed with deionised water (3 × 50 mL) and stored in deionised water (~10 mL) until further use. For sorption measurements, the obtained products were activated under vacuum (1×10^{-3} mbar) at 70 °C for 12 h.

Release of ThT from ThT@ZIF-8 and ThT@ZIF-8@Alg

In 50 mL falcon tubes, 10 mg ThT@ZIF-8 and or 60 mg ThT@ZIF-8@Alg beads (in wet state) were immersed in 10 mL of release medium (deionised water, PBS pH 7.4 or PBS pH 6). To obtain a PBS pH 6 solution, a PBS pH 7.4 solution was adjusted with 1 M HCl (aq.). The falcon tubes were placed in a shaking incubator (320 rpm) at 37 °C. After each hour, the release medium was completely exchanged, and the collected samples were adjusted to pH = 4 with 1 M HCl before UV/Vis

analysis (see ESI,† Section S2). Descriptions of other ThT release experiments can be found in the ESI† (Section S8).

Material characterisation

The PXRD measurements of as-prepared MOFs were performed on a *Rigaku* MiniFlex 600-C diffractometer with X-ray Cu Kα radiation (1.5406 Å) using Bragg–Brentano geometry. DR-UV/Vis spectra were recorded on a *Shimadzu* UV-3600i Plus Spectrophotometer. SEM images were recorded with a JEOL JSM-7500F High resolution field emission scanning electron microscope equipped with gentle beam mode. FTIR was measured with a PerkinElmer Frontier Spectrometer. UV/Vis spectra of liquids were recorded on an Agilent Technologies Cary 60. All characterization techniques are described in more detail in the ESI† (Section S1).

Cell culture maintenance

A549 lung cancer cells, and VERO E6 non-tumorigenic kidney cells were maintained in Dulbecco's modified Eagle's medium (high glucose, pyruvate, no glutamine), which was supplemented with heat-inactivated foetal bovine serum (qualified, South American origin, 10% v/v), gentamicin sulphate solution 50 mg mL^{-1} (1% v/v, 50 mg L^{-1} end concentration), and L-glutamine solution 200 nM (1% v/v, 2 nM end concentration) and were passaged twice a week. All reagents were purchased from Gibco™ at Thermo Scientific, and solvents from Sigma Aldrich if not stated differently. Ultrapure water (18.2 MΩ/0.56 μS at 25 °C) was provided by a BerryPure® mini from Berrytec. A549 and VERO E6 cells were obtained from Cell Line Service (CLS, Eppelheim, Germany).

Antiproliferative effects in cancerous and non-tumorigenic cells

A549 cells (6000 cells per well), or VERO E6 cells (8000 cells per well) were transferred to a flat-bottom 96-well microtiter plate and incubated at 37 °C/5% CO_2 for 24 h. Stock solutions of the compounds as suspensions in PBS (pH 7.4) were freshly prepared and diluted with the respective cell culture medium to increased concentrations ranging from 0–100 μg mL^{-1}. After 72 h of exposure, the cell culture medium was disposed, and the remaining cell biomass of living cells was quantified by 3-(4,5-dimethylthiazol-2-yl)-2,5-diphenyl tetrazolium bromide (MTT) (Sigma-Aldrich) staining and the absorptions were calculated as the delta of two measurements of the same well at wavelengths 570 (MTT) and 690 nm (background) by an Infinite 200pro® plate reader (Tecan). The EC_{50} values (half-maximal effective concentrations) were determined as the concentration that caused 50% inhibition of cell proliferation compared to untreated control (PBS in DMEM). The data represent the mean of three independent experiments.

Author contributions

SVD, JW, AC, RAF and RE conceived the concept and methodology. SVD, SD and TB conducted data collection, analysis, curation, and visualisation. KR and RE conducted SEM and TEM measurements. AC provided laboratory equipment for the release studies and biological insights. MC assisted with the cell culture studies and CS supervised the antiproliferative activity studies and analysed the data. SVD wrote the initial draft of the manuscript. JW, MZH, AC, RAF and RE supervised the work, reviewed, and edited the manuscript, and acquired funding support for the work. All authors reviewed and approved the final version of the manuscript.

Conflicts of interest

There are no conflicts to declare.

Data availability

The data supporting this article have been included as part of the ESI.† All data will be available *via* **https://mediatum.ub.tum.de**/after the acceptance.

Acknowledgements

SVD thanks Alexandros Tholiotis and Riccardo Scotti for initial experiments and support in the laboratory. SVD thanks Jürgen Kudermann for support with UV/Vis measurements and customisation of the incubator setup. Support from TUM's Innovation network project ARTEMIS is acknowledged. RE thanks the Fonds der Chemischen Industrie for a Liebig Fellowship.

Notes and references

1 J. Gao, J. M. Karp, R. Langer and N. Joshi, *Chem. Mater.*, 2023, **35**, 359–363.
2 M. W. Tibbitt, J. E. Dahlman and R. Langer, *J. Am. Chem. Soc.*, 2016, **138**, 704–717.
3 I. Álvarez-Miguel, B. Fodor, G. G. López, C. Biglione, E. S. Grape, A. K. Inge, T. Hidalgo and P. Horcajada, *ACS Appl. Mater. Interfaces*, 2024, **16**, 32118–32127.
4 C. Biglione, T. Hidalgo and P. Horcajada, *Drug Delivery Transl. Res.*, 2024, **14**, 2041–2045.
5 J. W. M. Osterrieth and D. Fairen-Jimenez, *Biotechnol. J.*, 2021, **16**, e2000005.
6 H. Furukawa, K. E. Cordova, M. O'Keeffe and O. M. Yaghi, *Science*, 2013, **341**, 1230444.
7 W. Cai, C.-C. Chu, G. Liu and Y.-X. J. Wáng, *Small*, 2015, **11**, 4806–4822.
8 X. Ma, M. Lepoitevin and C. Serre, *Mater. Chem. Front.*, 2021, **5**, 5573–5594.
9 Z. Sun, T. Li, T. Mei, Y. Liu, K. Wu, W. Le and Y. Hu, *J. Mater. Chem. B*, 2023, **11**, 3273–3294.
10 S. V. Dummert, H. Saini, M. Z. Hussain, K. Yadava, K. Jayaramulu, A. Casini and R. A. Fischer, *Chem. Soc. Rev.*, 2022, **51**, 5175–5213.
11 I. Abánades Lázaro, X. Chen, M. Ding, A. Eskandari, D. Fairen-Jimenez, M. Giménez-Marqués, R. Gref, W. Lin, T. Luo and R. S. Forgan, Metal–organic frameworks for biological applications, *Nat. Rev. Methods Primers*, 2024, **4**, 1–20.
12 H. D. Lawson, S. P. Walton and C. Chan, *ACS Appl. Mater. Interfaces*, 2021, **13**, 7004–7020.

13 M. Koshy, M. Spiotto, L. E. Feldman, J. J. Luke, G. F. Fleming, D. Olson, J. W. Moroney, R. Nanda, A. Rosenberg, A. T. Pearson, A. Juloori, F. Weinberg, C. Ray, R. C. Gaba, P. J. Chang, L. A. Janisch, Z.-Q. Xu, W. Lin, R. R. Weichselbaum and S. J. Chmura, *J. Clin. Orthod.*, 2023, **41**, 2527.
14 T. A. Tabish, M. Z. Hussain, R. A. Fischer and A. Casini, *Mater. Today*, 2023, **66**, 302–320.
15 C. Jeyaseelan, P. Jain, D. Soin and D. Gupta, *Inorg. Nano-Met. Chem.*, 2022, **52**, 1463–1475.
16 S. Mallakpour, E. Nikkhoo and C. M. Hussain, *Coord. Chem. Rev.*, 2022, **451**, 214262.
17 D. S. R. Khafaga, M. T. El-Morsy, H. Faried, A. H. Diab, S. Shehab, A. M. Saleh and G. A. M. Ali, *RSC Adv.*, 2024, **14**, 30201–30229.
18 A. Wang, M. Walden, R. Ettlinger, F. Kiessling, J. J. Gassensmith, T. Lammers, S. Wuttke and Q. Peña, *Adv. Funct. Mater.*, 2024, **34**, 2308589.
19 M. Mehta, T. A. Bui, X. Yang, Y. Aksoy, E. M. Goldys and W. Deng, *ACS Mater. Au*, 2023, **3**, 600–619.
20 A. K. Tewari, S. C. Upadhyay, M. Kumar, K. Pathak, D. Kaushik, R. Verma, S. Bhatt, E. E. S. Massoud, M. H. Rahman and S. Cavalu, *Polymers*, 2022, **14**, 3545.
21 Y. Ma, X. Qu, C. Liu, Q. Xu and K. Tu, *Front. Mol. Biosci.*, 2021, **8**, 805228.
22 N. T. T. Nguyen, T. T. T. Nguyen, S. Ge, R. K. Liew, D. T. C. Nguyen and T. van Tran, *Nanoscale Adv.*, 2024, **6**, 1800–1821.
23 M.-A. Gatou, I.-A. Vagena, N. Lagopati, N. Pippa, M. Gazouli and E. A. Pavlatou, *Nanomaterials*, 2023, **13**, 2224.
24 A. Raza and W. Wu, Metal-organic frameworks in oral drug delivery, *Asian J. Pharm. Sci.*, 2024, **19**, 100951.
25 S. Javanbakht, A. Hemmati, H. Namazi and A. Heydari, *Int. J. Biol. Macromol.*, 2020, **155**, 876–882.
26 S. Javanbakht, M. Pooresmaeil, H. Hashemi and H. Namazi, *Int. J. Biol. Macromol.*, 2018, **119**, 588–596.
27 Y. Zeng, C. Zhang, D. Du, Y. Li, L. Sun, Y. Han, X. He, J. Dai and L. Shi, *Acta Biomater.*, 2022, **145**, 43–51.
28 Y. Zhou, L. Liu, Y. Cao, S. Yu, C. He and X. Chen, *ACS Appl. Mater. Interfaces*, 2020, **12**, 22581–22592.
29 Y. Liu, N. Ma, N. Gao, G. Ling and P. Zhang, *J. Drug Delivery Sci. Technol.*, 2022, **75**, 103604.
30 A. G. Márquez, T. Hidalgo, H. Lana, D. Cunha, M. J. Blanco-Prieto, C. Álvarez-Lorenzo, C. Boissière, C. Sánchez, C. Serre and P. Horcajada, *J. Mater. Chem. B*, 2016, **4**, 7031–7040.
31 S. Mansi, S. V. Dummert, G. J. Topping, M. Z. Hussain, C. Rickert, K. M. A. Mueller, T. Kratky, M. Elsner, A. Casini, F. Schilling, R. A. Fischer, O. Lieleg and P. Mela, *Adv. Funct. Mater.*, 2024, **34**, 2304907.
32 M. Gao, C. Yang, C. Wu, Y. Chen, H. Zhuang, J. Wang and Z. Cao, *J. Nanobiotechnol.*, 2022, **20**, 404.
33 E. M. Ahmed, *J. Adv. Res.*, 2015, **6**, 105–121.
34 J. Y. C. Lim, L. Goh, K.-I. Otake, S. S. Goh, X. J. Loh and S. Kitagawa, *Biomater. Sci.*, 2023, **11**, 2661–2677.
35 J. Xiao, S. Chen, J. Yi, H. Zhang and G. A. Ameer, *Adv. Funct. Mater.*, 2017, **27**, 1604872.
36 H. Liu, H. Peng, Y. Xin and J. Zhang, *Polym. Chem.*, 2019, **10**, 2263–2272.
37 S. L. Tomić, M. M. Babić Radić, J. S. Vuković, V. V. Filipović, J. Nikodinovic-Runic and M. Vukomanović, *Mar. Drugs*, 2023, **21**, 177.
38 M. Z. I. Mollah, H. M. Zahid, Z. Mahal, M. R. I. Faruque and M. U. Khandaker, *Front. Mol. Biosci.*, 2021, **8**, 719972.
39 D. R. Sahoo and T. Biswal, *SN Appl. Sci.*, 2021, **31**–19.
40 H. H. C. de Lima, C. T. P. Da Silva, V. L. Kupfer, J. de, C. Rinaldi, E. S. Kioshima, D. Mandelli, M. R. Guilherme and A. W. Rinaldi, *Carbohydr. Polym.*, 2021, **251**116977.
41 Y. Lin, Y. Sun, Y. Dai, W. Sun, X. Zhu, H. Liu, R. Han, D. Gao, C. Luo and X. Wang, *Talanta*, 2020, **207**, 120300.
42 Y. Yu, G. Chen, J. Guo, Y. Liu, J. Ren, T. Kong and Y. Zhao, *Mater. Horiz.*, 2018, **5**, 1137–1142.
43 M. Zhang, G. Wang, D. Wang, Y. Zheng, Y. Li, W. Meng, X. Zhang, F. Du and S. Lee, *Int. J. Biol. Macromol.*, 2021, **175**, 481–494.
44 K. S. Park, Z. Ni, A. P. Côté, J. Y. Choi, R. Huang, F. J. Uribe-Romo, H. K. Chae, M. O'Keeffe and O. M. Yaghi, *Proc. Natl. Acad. Sci. U. S. A.*, 2006, **103**, 10186–10191.
45 H. Zhang, D. Liu, Y. Yao, B. Zhang and Y. S. Lin, *J. Membr. Sci.*, 2015, **485**, 103–111.
46 R. Ettlinger, U. Lächelt, R. Gref, P. Horcajada, T. Lammers, C. Serre, P. Couvreur, R. E. Morris and S. Wuttke, *Chem. Soc. Rev.*, 2022, **51**, 464–484.
47 R. Ricco, P. Wied, B. Nidetzky, H. Amenitsch and P. Falcaro, *Chem. Commun.*, 2020, **56**, 5775–5778.
48 H. Kaur, G. C. Mohanta, V. Gupta, D. Kukkar and S. Tyagi, *J. Drug Delivery Sci. Technol.*, 2017, **41**, 106–112.
49 Q. Wang, Y. Sun, S. Li, P. Zhang and Q. Yao, *RSC Adv.*, 2020, **10**, 37600–37620.
50 B. S. Padya, G. Fernandes, S. Hegde, S. Kulkarni, A. Pandey, P. B. Deshpande, S. F. Ahmad, D. Upadhya and S. Mutalik, *Pharmaceutics*, 2023, **15**, 2594.
51 C. Xue, T. Y. Lin, D. Chang and Z. Guo, *R. Soc. Open Sci.*, 2017, **4**, 160696.
52 S. Sarkar, J. Raymick, B. Ray, D. K. Lahiri, M. G. Paule and L. Schmued, *Curr. Alzheimer Res.*, 2015, **12**, 837–846.
53 M. Biancalana and S. Koide, *Biochim. Biophys. Acta*, 2010, **1804**, 1405–1412.
54 A. A. Maskevich, V. I. Stsiapura, V. A. Kuzmitsky, I. M. Kuznetsova, O. I. Povarova, V. N. Uversky and K. K. Turoverov, *J. Proteome Res.*, 2007, **6**, 1392–1401.
55 H. Zheng, Y. Zhang, L. Liu, W. Wan, P. Guo, A. M. Nyström and X. Zou, *J. Am. Chem. Soc.*, 2016, **138**, 962–968.
56 W. Morris, C. J. Stevens, R. E. Taylor, C. Dybowski, O. M. Yaghi and M. A. Garcia-Garibay, *J. Phys. Chem. C*, 2012, **116**, 13307–13312.
57 E. V. Hackl, J. Darkwah, G. Smith and I. Ermolina, *Eur. Biophys. J.*, 2015, **44**, 249–261.
58 R. B. Cundall, A. Davies, P. G. Morris and J. Williams, *J. Photochem.*, 1981, **17**, 369–376.
59 V. Foderà, M. Groenning, V. Vetri, F. Librizzi, S. Spagnolo, C. Cornett, L. Olsen, M. van de Weert and M. Leone, *J. Phys. Chem. B*, 2008, **112**, 15174–15181.
60 A. Paul, I. K. Banga, S. Muthukumar and S. Prasad, *ACS Omega*, 2022, **7**, 26993–27003.

61 Y. Pan, D. Heryadi, F. Zhou, L. Zhao, G. Lestari, H. Su and Z. Lai, *CrystEngComm*, 2011, **13**, 6937.
62 F. Yang, H. Mu, C. Wang, L. Xiang, K. X. Yao, L. Liu, Y. Yang, Y. Han, Y. Li and Y. Pan, *Chem. Mater.*, 2018, **30**, 3467–3473.
63 M. Groenning, *J. Chem. Biol.*, 2010, **3**, 1–18.
64 B. Xu, Y. Mei, Z. Xiao, Z. Kang, R. Wang and D. Sun, *Phys. Chem. Chem. Phys.*, 2017, **19**, 27178–27183.
65 S. Brunauer, L. S. Deming, W. E. Deming and E. Teller, *J. Am. Chem. Soc.*, 1940, **62**, 1723–1732.
66 S. Yang, L. Peng, O. A. Syzgantseva, O. Trukhina, I. Kochetygov, A. Justin, D. T. Sun, H. Abedini, M. A. Syzgantseva, E. Oveisi, G. Lu and W. L. Queen, *J. Am. Chem. Soc.*, 2020, **142**, 13415–13425.
67 H. Zhu, Q. Zhang and S. Zhu, *ACS Appl. Mater. Interfaces*, 2016, **8**, 17395–17401.
68 R. He, J. He, J. Shen, H. Fu, Y. Zhang and B. Wang, *Soft Sci.*, 2024, **4**, 37.
69 M. d J. Velásquez-Hernández, R. Ricco, F. Carraro, F. T. Limpoco, M. Linares-Moreau, E. Leitner, H. Wiltsche, J. Rattenberger, H. Schröttner, P. Frühwirt, E. M. Stadler, G. Gescheidt, H. Amenitsch, C. J. Doonan and P. Falcaro, *CrystEngComm*, 2019, **21**, 4538–4544.
70 H. Malektaj, A. D. Drozdov and J. deClaville Christiansen, *Polymers*, 2023, **15**, 3012.
71 D. Massana Roquero, A. Othman, A. Melman and E. Katz, *Mater. Adv.*, 2022, **3**, 1849–1873.

